Role of Zn in aluminosilicate glasses used as supplementary cementitious materials

Mingione, Serena; Pedersen, Malene Thostrup; Sørensen, Søren Strandskov; Winnefeld, Frank; Montagnaro, Fabio; Yue, Yuanzheng

Published in:
Journal of Non-Crystalline Solids

DOI (link to publication from Publisher):
10.1016/j.jnoncrysol.2023.122397

Publication date:
2023

Document Version
Publisher's PDF, also known as Version of record

Journal of Non-Crystalline Solids 614 (2023) 122397

Contents lists available at ScienceDirect

Journal of Non-Crystalline Solids

journal homepage: www.elsevier.com/locate/jnoncrysol

Role of Zn in aluminosilicate glasses used as supplementary cementitious materials

Serena Mingione [a,b,*], Malene T. Pedersen [a,c,*], Søren S. Sørensen [d], Frank Winnefeld [a], Fabio Montagnaro [b], Yuanzheng Yue [d]

[a] Empa Swiss Federal Laboratories for Materials Science and Technology, Laboratory for Concrete and Asphalt, 8600 Dübendorf, Switzerland
[b] Department of Chemical Sciences, University of Naples Federico II, Complesso Universitario di Monte Sant'Angelo, 80126 Naples, Italy
[c] Norwegian University of Science and Technology (NTNU), Department of Structural Engineering, Trondheim 7491, Norway
[d] Department of Chemistry and Bioscience, Aalborg University, 9220 Aalborg, Denmark

ARTICLE INFO

Keywords:
Glass
Blast furnace slag
Supplementary cementitious materials
Zinc
Reactivity

ABSTRACT

The cement industry relies on the use of supplementary cementitious materials (SCM) to lower the related CO_2 emission. SCM are often amorphous materials containing minor elements, which is why it is important to study the impact of these materials on cement reactivity. Two calcium aluminosilicate glass series as model substances of SCM were synthesized and investigated. In both series Ca was partially replaced by Zn, Sr and Mg in different ratios. Moreover, four cement blends made with CEM I 52.5 R and aqueous solutions of $Mg(NO_3)_2{\cdot}6H_2O$, $Zn(NO_3)_2{\cdot}6H_2O$ and $Sr(NO_3)_2$ were investigated. Zn retards the reactivity of both glasses and cements system. This retardation effect is suggested to be related both to the formation of the calcium hydroxozincate hydrate, which affects the portlandite formation and, thus, the pH of the system, and to the formation of surface complexes which retards the dissolution and so the reactivity of the glasses.

1. Introduction

Concrete is the most widely used building material in the world today, with an estimated yearly consumption approaching 30 billion tons [1]. Consequently, concrete production has a significant CO_2 footprint. The reactive component in concrete is Portland cement (PC), for which the production is associated with a generation of about 0.85 kg CO_2/kg clinker [1–4]. The total CO_2 emissions generated by the cement industry constitute to at least 5% of the total anthropogenic CO_2 emissions [5]. A possible solution to reduce the CO_2 emissions from clinker production is the partial replacement of clinker with supplementary cementitious materials (SCM) bearing low-CO_2 emissions. Generally, SCM are industrial wastes that react with pozzolanic or hydraulic features, such as fly ash (FA), ground granulated blast furnace slag (GGBFS), and silica fume; but also calcined clays and natural pozzolans are now used to an increasing extent [6,7]. These materials find applications in concrete, either in blended cements or added separately in the concrete mixer, replacing a portion of the PC in concrete (typically in the order of 10-50% [6]). In this way, the amount of clinker used in concrete is reduced.

Using less clinker has numerous economic and environmental benefits such as lower consumption of natural raw materials (limestone and clay), less use of fuel, which means lower production of effluent gasses, and in particular less production of CO_2 from both fuel combustion and calcination of $CaCO_3$. FA and GGBFS represent the majority of SCM currently used, but their use as SCM is limited by supply and demand concerns, and cost of transportation. The annual global production of FA and GGBFS today is approximately 1 billion tonnes and 360 million tonnes, respectively, while the cement demand is projected to rise to 5.8 billion tonnes by 2050 [8]. Therefore, fly ash and ground granulated blast furnace slag can only partially satisfy this rising demand for SCM. For that, the focus of much of the recent research on SCM has been on the exploration of alternative SCM and their performance in concrete. Alternative SCM are often based on industrial by-products locally available such as non-ferrous slags, steel slags, by-products from ferro-silicon alloy processes, and incinerator or co-combustion ashes [9,10]. Also CAS ($CaO\text{-}Al_2O_3\text{-}SiO_2$) and NCAS ($Na_2O\text{-}CaO\text{-}Al_2O_3\text{-}SiO_2$) glasses can be used as alternative SCM. Their production is normally based on local materials and results in a CO_2 emission less than 60% respect to that emitted from Portland cement production [11,12]. The

* Corresponding authors.
E-mail addresses: serena.mingione@empa.ch (S. Mingione), malene.t.pedersen@ntnu.no (M.T. Pedersen).

https://doi.org/10.1016/j.jnoncrysol.2023.122397
Received 15 February 2023; Received in revised form 24 April 2023; Accepted 15 May 2023
Available online 26 May 2023

advantages of using locally available materials include lower costs and less problems concerning the transportation. Furthermore, the use of by-products allows for a sustainable system loop that can convert the valuable resources which are usually treated as waste materials, and e.g. landfilled, into useful products [9,13].

A slag that has already proven useful comes from the ferroalloy production. Usually, ferrous slag mainly contains Ca and Si with other major elements like Mg and Al [14]. Though most ferroalloy slags are currently landfilled, a small proportion is treated for application in inner plant recycling and cement mixtures [13]. One of the slags, which can be used as alternative SCM, is the electric arc furnace ferronickel slag, as a residue generated in the ferronickel alloy production process via melting of laterite ore in an electric arc furnace at 1500-1600°C. This slag has been used for replacement up to 20 wt.% clinker. However, some of the other alternative slags of interest as SCM show a limited pozzolanic reactivity and thereby a limited contribution to the compressive strength of cement. This is usually due to the low content of calcium oxide that cannot satisfy the setting time and the concrete strength required for civil engineering applications [15]. Often also minor elements are present, which influence the reactivity of both SCM and cement [7]. Alternative slags of interest as SCM are known to contain heavy metals [10]. The removal process of these elements is usually challenging and incomplete and, to advance in the usage of alternative slags as SCM, it is important to thoroughly understand the impact of heavy metals and other minor elements on both the slag and cement reactivity [10]. This is the scope of the current study. Compared to GGBFS, the alternative slags often have a significantly higher Fe content, and a lower Ca content. The high Fe content has been the topic of recent studies [16,17]. To distinguish the impact of minor elements from that of iron, calcium aluminosilicates were chosen as model systems, which resemble the composition of GGBFS. In these systems, Ca^{2+} was substituted by different divalent ions (Zn^{2+}, Sr^{2+}, Mg^{2+}) in the alternative slags.

Specifically, two glass series were synthesized and investigated. In the first series, increasing amounts of Ca were substituted by Zn to elucidate the role of Zn in slag. Zinc is often present in alternative slags, especially non-ferrous-slags [14]. Studies on those slags are scarce in literature since their production is very low, however they can still be useful as local SCM [17,18]. Therefore, Zn is of special interest in this study. In the second series, Ca^{2+} was partially replaced by Mg^{2+}, Zn^{2+}, and Sr^{2+} in different ratios, with the aim to understand how divalent ions of different cation field strength (CFS) influence the glass structure and reactivity, and if the role of Zn is affected by the presence of other divalent ions. The CFS is the ratio of the formal charge of the cation to the cation-oxygen bond distance squared [19]. It is used to control the ordering process in a glass of the elements which tend to compete for certain preferred site and coordination state to lower the total free energy of the system. The characteristics of the synthesized glasses were studied using X-ray diffraction (XRD) and differential scanning calorimetry (DSC), while the reactivity of the glasses was elucidated by dissolution tests in alkaline solutions and reactivity with $Ca(OH)_2$ in a pozzolanic test [20]. Moreover, the effect of the divalent ions on the cement hydration was investigated by isothermal calorimetry, XRD, and thermogravimetric analysis (TGA) [20].

2. Materials and methods

2.1. Glass synthesis and crystallization experiments

Nine glasses within the CaO-Al_2O_3-SiO_2 (CAS) system were prepared to obtain two glass series. The first series involves five glasses with the targeted composition $(50-x)CaO$-$xZnO$-$10Al_2O_3$-$40SiO_2$, x={0,10,20,30,40}, constituting the Zn-series. The second series involves four glasses containing mixed divalent cations, i.e., with the targeted composition $(50-x-y-z)CaO$-$xZnO$-$ySrO$-$zMgO$-$10Al_2O_3$-$40SiO_2$, x={0,10,15,30}, y={0,10,15,0}, z={0,10,0,0}, constituting the mixed-series. The compositions of Ref I and Ref II, prepared with x, y, z=0, resemble those of the blast furnace slag and serve as references for this work. The chemical compositions of the glasses were determined by X-ray fluorescence analyses as listed in Tables 1 and 2, respectively, along with the number of non-bridging oxygen per tetrahedron (NBO/T) calculated as:

$$\frac{NBO}{T} = \frac{2\cdot(CaO + MgO + SrO + ZnO)}{(SiO_2 + Al_2O_3)} \quad (1)$$

NBO/T is a measure of structural network connectivity, and it was corrected by subtraction of the crystalline part for the Zn-series glasses [20,21]. A higher NBO/T value means a lower structural network connectivity.

The two series of glasses were synthesized in two different laboratories. For each of the compositions in the Zn-series [22], powder mixtures of $CaCO_3$, Al_2O_3, SiO_2, $ZnCO_3$, and Na_2CO_3 were homogenized before synthesis, targeting minimum 200 g of bulk glass. The powder mixture was subsequently melted in a Pt/Rh 90/10 crucible using an electric furnace (ENTECH, Sweden). The crucible with the powder was inserted into the furnace at 1500°C and kept at this temperature for 1.5 h. The temperature was lowered to 1400°C, and the melt was swirled in the crucible before being cast onto a brass plate in order to obtain pure glassy materials. Half of the casted melt was annealed at 750°C for 10 min. The annealed glasses were used for DSC analysis and therefore cut into thin slices using a Struers Secotom 10 instrument with a wheel speed of 1200 rpm and a feed-speed of 0.085 mm/s. During cutting, the metal blade and sample were flushed with water to prevent dust. The slices were formed into disc-like pieces by grinding with 30 and 320 grit SiC grinding paper [22].

For the synthesis of the mixed-series, CaO, SiO_2, Al_2O_3, Na_2CO_3, ZnO, $SrCO_3$ and MgO were weighed to obtain 100 g glass with the desired composition. The powders were homogenized by continuous tumbling for 2 h. For each sample, the mixture of oxides was heated in an electric furnace (Carbolite GERO) to 950°C (5 K/min), then maintaining the mixture at the maximum temperature for 15 min to ensure the release of carbonates. The mixture was then heated to 1450°C (10 K/min) and kept for 3 h before raising again the temperature up to 1600°C (2 K/min), where the sample was kept for 1 h. The oven was then cooled to a temperature of 1450°C (5 K/min) and the glass was quenched in water to ensure the formation of amorphous material. Each glass was rinsed with isopropanol and kept in a desiccator under vacuum until analysis.

The non-annealed glasses in both series were ground in a ball mill (Retsch PM 100) in steps of 2 min, until a particle size <63 μm was obtained. For the reactivity tests, particles in the size range 40-63 μm were used ("medium-sized samples"), whereas particles <40 μm ("fine-sized samples") were used for characterization of the glass structure. The particle size distributions (Fig. S.1) were measured on a Malvern Mastersizer X laser granulometer, using a 300 μm lens and isopropanol as dispersant. For both glass series the median of the particle size distribution (d_{50}) is reported in Table 1 and Fig. S.1 (in supplementary materials), respectively.

Finally, a piece of each annealed glass from the Zn-series was heat-treated at 1100°C for 4 h in a muffle furnace. Then, the furnace was turned off and the glass samples were left to cool to room temperature in the closed furnace overnight. The heat-treated samples were ground as described above and subjected to XRD measurements. In addition, about 1.5 g of glass of the mixed-series was crystalized by keeping at 850°C in a muffle furnace for 6 h.

2.2. Cement systems

Isothermal calorimetry

To investigate the effect of zinc ions on the early hydration kinetics of cement, four cement blends were prepared and measured by isothermal calorimetry. All blends were prepared with a CEM I 52.5 R cement (Table S.1) and mixed with $Zn(NO_3)_2{\cdot}6H_2O$ dissolved in demineralized

Table 1
Chemical composition for the glasses (mol%) in the Zn-series as determined by X-ray fluorescence (XRF) analysis and corrected by the presence of crystalline phase, with values for NBO/T and d_{50}.

Name	Targeted composition	CaO	Al_2O_3	SiO_2	ZnO	Other[a]	NBO/T	d_{50} [μm]
Ref I	$50CaO10Al_2O_340SiO_2$	51.3	10.0	38.5	0.1	0.1	2.12	30.3
Zn10	$10ZnO40CaO10Al_2O_340SiO_2$	41.4	9.9	38.2	10.1	0.5	2.14	23.0
Zn20	$20ZnO30CaO10Al_2O_340SiO_2$	31.0	9.7	37.8	20.4	1.0	2.16	47.2
Zn30	$30ZnO20CaO10Al_2O_340SiO_2$	20.6	9.4	37.8	30.6	1.6	2.17	44.3
Zn40	$40ZnO10CaO10Al_2O_340SiO_2$	10.7	10.3	40.6	36.3	2.1	1.84	37.5

[a] Traces of Na_2O, P_2O_5, Fe_2O_3, K_2O, MgO, and SO_3 were detected

Table 2
Chemical composition for the glasses (mol%) in the mixed-series as determined by XRF analysis, with values for NBO/T and d_{50}.

Name	Targeted composition	CaO	Al_2O_3	SiO_2	ZnO	SrO	MgO	Other[a]	NBO/T	d_{50} [μm]
Ref II	$50CaO10Al_2O_340\ SiO_2$	48.4	10.3	41.0				0.4	1.88	17.2
Zn	$xZnO20CaO10Al_2O_340SiO_2$[b]	25.9	6.5	32.0	35.4			0.3	3.18	35.8
ZnSr	$xZnOySrO20CaO10Al_2O_340SiO_2$[b]	21.7	7.5	36.8	17.6	16.1		0.4	2.50	30.6
ZnSrMg	$xZnOySrOzMgO20CaO10Al_2O_340SiO_2$[b]	24.0	8.4	40.7	9.1	8.1	9.6	0.2	2.07	65.4

[a] Traces of Na_2O, P_2O_5, Fe_2O_3, K_2O, MgO, and SO_3 were detected
[b] x={30,15,10}, y={0,15,10}, z={0,0,10}

water, giving zinc concentrations in the mixing water of 0, 14.5, 29, and 58 mM resembling Zn released from different slag into pore solution. 6 g of paste, with a composition of of 0, 0.16, 0.32 and 0.63 g Zn/g cement, respectively. The pastes were mixed externally (500 rpm) for 2 min using an electric stirrer, and isothermal calorimetry measurements were carried out at 20°C for 7 days using a TAM Air (TA Instruments) apparatus.

Preparation of cement pastes

The influence of Zn, Sr and Mg ions on cement hydration was investigated using three blends. The first blend contained CEM I 52.5 R and $Mg(NO_3)_2{\cdot}6H_2O$, $Zn(NO_3)_2{\cdot}6H_2O$ and $Sr(NO_3)_2$ dissolved in demineralized water, as shown in Table 3. The ion concentrations were based on those expected in a system containing 30 wt.% of the prepared glasses in the mixed-series and 70 wt.% cement with w/c=0.71, assuming a glass reaction degree of 20%. This reaction degree is consistent with earlier studies [20]. A reference sample was prepared by mixing demineralized water and cement with w/c=0.71. Each sample was mixed individually with a spatula for 2 min, transferred to 15 mL centrifuge tubes and sealed. The samples were stored at 20°C; they were kept on a rolling board for the first 48 h to avoid segregation. At each hydration time (2, 7, 14, 28 and 91 d), the samples were fractured, and the hydration was stopped by solvent exchange with isopropanol [23]. The samples were crushed and submerged first in isopropanol for 20 min, and then in polyethylene ether for 10 min. The samples were subsequently dried at 40°C for 5 min. TGA and XRD characterizations were then carried out.

2.3. X-ray diffraction (XRD) analyses

XRD measurements were conducted on a PANalytical X'Pert Pro instrument with Bragg-Brentano geometry and equipped with an X'Celerator detector using CoK_α radiation. Voltage and current were 45 kV and 40 mA, respectively, and the measurement range was 2θ=5-90°. For measurements on the glasses after synthesis, the following settings were used: mask of 10 mm, fixed divergence slit of ¼°, anti-scatter slit of ½° and measurement time of 90 min. For the crystallization experiments, the following setting were used: mask 20 mm, fixed divergence slit 1/8° and anti-scatter slit ¼°. The hydrated cement samples were scanned for 45 min using a mask of 15 mm, an anti-scatter slit of 1°, divergence slit of ½°, and the same 2θ scanning range as used for the glasses. Rietveld refinement was performed using the X'Pert HighScore Plus 3.0e software, and the external standard method [24,25] was utilized with CaF_2. The crystal structures used for the refinement are taken from Snellings [26] if not reported separately in the supplementary materials (Table S.2).

Table 3
Solutions prepared for cement hydration studies. The weighed nitrates were mixed with 200 mL demineralized water.

Solution	$Zn(NO_3)_2{\cdot}6H_2O$		$Sr(NO_3)_2$		$Mg(NO_3)_2{\cdot}6H_2O$	
	[g]	g Zn/g cement	[g]	g Sr/g cement	[g]	g Mg/g cement
Zn	30.68	0.024	-	-	-	-
Zn-Sr	14.65	0.011	10.42	0.015	-	-
Zn-Sr-Mg	10.52	0.008	7.48	0.011	9.06	0.003

2.4. Thermogravimetric analyses (TGA)

TGA was executed using a Mettler Toledo TGA/SDTA851e instrument. Approximately 50 mg sample was investigated in the temperature range 30–980°C with a heating rate of 20 K/min under an N_2 atmosphere. The detected mass loss was corrected with the mass loss of an empty pan measured prior to each series of analyses. The amount of Ca $(OH)_2$ in the samples was calculated.

2.5. Different scanning calorimetry (DSC) analyses

DSC was performed on a Netzsch STA 449 F1 Jupiter instrument in a Pt crucible with lid. The sample was measured under an argon flow rate of 50 mL/min and protective gas (Ar) flow rate of 20 mL/min. The heating and cooling rates were 20 K/min. To assess the glass transition temperatures (T_g) and the thermal response of the zinc-series glasses, single up-scans were conducted from 50 to 1000°C on one of the prepared discs for each glass.

2.6. ^{27}Al and ^{29}Si NMR analyses

^{27}Al magic angle spinning (MAS) nuclear magnetic resonance (NMR) spectra of the Zn-series were recorded on a Varian Direct-Drive-600 spectrometer with a magnet strength of 14.09 T, using a home-built CP/MAS probe for 4 mm o.d. partially stabilized zirconia rotors. The NMR measurements were run with a pulse width of 0.5 μs, spinning speed of 13 kHz, relaxation delay of 1 s, and using 1 M $AlCl_3{\cdot}6H_2O$ (aq) as chemical shift reference [22]. ^{27}Al MAS NMR spectra of the mixed-series were obtained with a Bruker Avance III NMR instrument

with a pulse width of 1 μs, relaxation delay of 1 s, magnetic field strength of 9.4 T, a 2.5 mm probe and a spinning speed of 25 kHz. The ^{27}Al NMR chemical shifts were referred to a 1.1 M solution of $Al(NO_3)_3$ in D_2O. The ^{27}Al MAS NMR spectra were analyzed using the DMFIT program [27] where lineshapes were reproduced using the CzSimple model [28]. The CzSimple model is a version of the Czjzek distribution of quadrupolar interaction for the distribution of the isotropic chemical shift (Gaussian isotropic model, GIM, for d=5) with an uncoupled distribution of isotropic chemical shift, where the GIM corresponds to a statistical distribution of charges around the observed nucleus. Using the CzSimple model allows for optimal spectral simulation by varying the quadrupolar coupling constant, isotropic chemical shift (δ_{iso}) and the Gaussian distribution of δ_{iso} [29]. For both the zinc- and the mixed-series, ^{29}Si MAS NMR measurements were performed on the Bruker Avance III NMR spectrometer with a pulse width of 2.50 μs, relaxation delay of 30 s, magnetic field strength of 9.4 T, a 7 mm CP/MAS probe and spinning speed of 4.5 kHz. The ^{29}Si chemical shifts were referred to tetramethylsilane.

2.7. Reactivity tests

Dissolution tests

The reactivities of the synthesized glasses were investigated by dissolution tests, following the procedure described by Schöler et al. [20]. 0.1 g of glass powder (40-63 μm) was mixed with 100 g of 0.3 M KOH solution and kept in a PET vessel at a rocking table at 20°C until measurement. A sample was prepared for each selected time: 0.5, 1, 2, 4 and 8 h. At the corresponding time, 15 mL of the solution was collected in a syringe and filtered through a 0.45 μm nylon filter. Each sample was then diluted by a factor of 1:2, 1:5 and 1:10 using 2% ultra-pure HNO_3 solution. The concentrations of Si, Al, Ca, Zn Sr and Mg were determined from inductively coupled plasma-optical emission spectrometry (ICP-OES) analysis utilizing an ICP-OES MY19451002 instrument with a plasma flow of 12 L/min and a nebulizer flow of 0.7 L/min. All glasses were observed to dissolve congruently. As done in other studies [20,30], the dissolution degree of the glasses was calculated by using Al as a tracer of the dissolution kinetics.

Considering that the dissolution of a glass particle depends on both the particle specific surface area and the structure of the glass (network connectivity), the dissolution degree was normalized by the particles mean diameter (d_{50}) and the fraction of non-bridging oxygen per tetrahedron, NBO/T, (Eq. (1)):

$$X_{Al}[wt.\ \%/\mu m] = \frac{w_{Al\ rel}}{w^0_{Al\ glass}} \cdot \frac{100}{\frac{NBO}{T} \cdot d_{50}} \quad (2)$$

Where $w_{Al\ rel}$ represent the amount in mass [g] of Al released in the solution during the hydration time, and $w^0_{Al\ glass}$ is the amount in mass [g] of Al in the glass before the dissolution test. It is known that the specific surface area of a particle is related to his diameter, the bigger is the particle the smaller is the specific surface area and vice versa. A small specific surface area decreases the dissolution of the particle. The dissolution degree was normalized for the mean diameter of the particles as the effect of the different particle sizes between each glasses, and so of the specific surface area, was visible among the results. In this way it was possible to look only at the effect of the different divalent ions on the dissolution of the glasses.

Pozzolanity tests

The pozzolanic reactivity of the glasses was investigated in model systems consisting of 55.7 wt.% glass (40-63 μm), 38.8 wt.% $Ca(OH)_2$, 5.5 wt.% $CaCO_3$ as dry mix, and 0.3 M KOH, simulating a cementitious environment. 1.3 g of dry mix was blended with 1.3 g of 0.3 M KOH solution (w/s=1). A sample was prepared for each hydration time (1, 2, 7, 14, 28, 56, 91 and 182 days) and, at the chosen times, the hydration was stopped by solvent exchange (see Section 2.2). The dried samples were analyzed by TGA. The mass loss associated with the decomposition of portlandite was identified as the peak around 450°C, and the amount of portlandite was correspondingly calculated and expressed as percentage of the sample mass at 550°C.

3. Results and discussion

3.1. Glass structure

For the Zn-series, the analysis by XRD verify that the glasses have a primarily amorphous structure, though minor amounts of crystalline phases are present (see Fig. S.2 in the Supplementary Materials (SM)). Ref I contains a small percentage of quartz, Zn10 contained 1.7 wt. % gehlenite, Zn30 contains 0.6 wt. % zinc aluminum oxide, and Zn40 contains 12.1 wt. % zinc silicate and 0.3 wt. % zinc aluminum oxide (see Table S.2 in supplementary materials for references to the crystal structures used in the refinements). For the mixed-series, the XRD measurements confirm completely amorphous materials (Fig. S.3). The difference in crystallinity observed between the two series is assigned to the different synthesis processes. As the mixed-series experienced a faster quenching, amorphous materials were obtained also for the high Zn containing composition (30 mol. %).

The ^{27}Al NMR spectra of the Zn-series show how the substitution of Ca by Zn leads to a systematic shift of δ_{iso} towards lower frequency with increasing Zn fraction (Fig. 1a and Table S.3), indicating a change in the Al environment. This change is suggested to result from a gradual increase in Zn acting to compensate $[AlO_4]^-$ charge, as the Ca/Zn ratio decreases in the glass. Asymmetric center bands with a tail towards lower frequency are observed for all glasses, which reflects that the amorphous character of the material can result in a distribution of electric field gradients for the Al sites [31,32]. In the case of five-fold coordinated Al, it would appear in the same region as the tail is observed, thus no clear indication for Al(V) can be given. Moreover, ^{27}Al MAS NMR reveal the presence of six-fold coordinated aluminum around 20 ppm in the Zn30 and Zn40 glasses, consistent with the formation of Zn_2AlO_4. The formation of Zn_2AlO_4 indicates that Zn and Al are in close proximity in the glass, which is consistent with Zn acting to compensate $[AlO_4]^-$ charge when it is present in high amounts.

Comparing the ^{27}Al NMR spectra of the glasses in the mixed-series (Fig. 1b), a decrease in δ_{iso} is observed in the order (Zn)=(Ref II)> (ZnSr)=(ZnSrMg). The difference in chemical shift is related to the change in charge compensating ions for $[AlO_4]^-$ [33]. In the Ref II glass, Ca^{2+} is the only modifier that is charge-compensating $[AlO_4]^-$, and binds to NBO-containing $[SiO_4]$ tetrahedra. In the Zn glass, both Ca^{2+} and Zn^{2+} are present in the glass, but the similar δ_{iso} to Ref II suggests that Zn is not a charge-compensator of $[AlO_4]^-$. This is different from the Zn-series, where a shift to lower frequencies is observed for the Zn30 glass, which has a comparable composition to the Zn glass in the mixed-series. This difference may be explained by the different synthesis procedures. Additional modifier ions are present in the ZnSr and ZnSrMg glasses, and the shift in δ_{iso} indicates a change in the environment around Al and, thus, a change in the charge compensating ion. The role of the modifying ions is generally explained by their cation field strength (CFS), and it is expected that ions with a higher value of CFS bind to NBO-containing SiO_2 tetrahedra, while the ions with a lower value of CFS compensate $[AlO_4]^-$ [34,35]. The CFS decreases in the order Zn^{2+}>Mg^{2+}>Ca^{2+}>Sr^{2+}, hence Sr^{2+} is expected to be the main charge balancing cation in the ZnSr and ZnSrMg glasses. Sr^{2+} has the lowest electronegativity and the highest atomic number of divalent ions, which is consistent with a higher shielding effect and thus the lower δ_{iso} observed for the ZnSr and ZnSrMg glasses. Thereby we observe no change in the role of Zn neither as a result of the changing Zn content in the mixed series glasses nor as a result of the incorporation of Sr and/or Mg at a total substitution degree of 30 mol%.

It should be stated that only very small changes are observed in ^{27}Al MAS NMR line shapes and chemical shifts for both series, indicating that

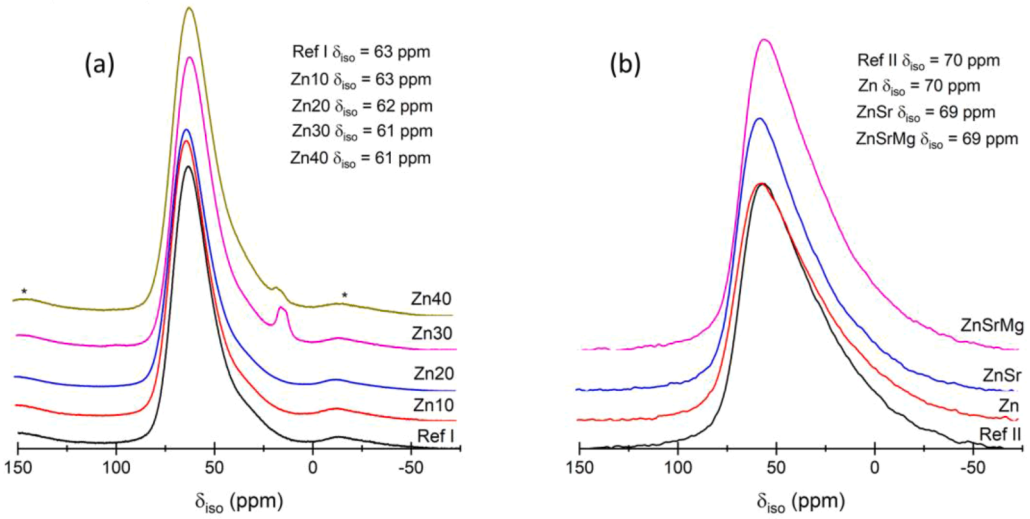

Fig. 1. ^{27}Al MAS NMR spectra for the glasses in the (a) Zn-series [22] (14.09 T) and (b) mixed-series (9.4 T). Intensities have been normalized for the weight percentage of Al contained in each glass. * = spinning sideband.

the substitution of the different divalent ions (Zn^{2+}, Sr^{2+}, Mg^{2+}) for the Ca^{2+} does not cause any detectable changes in the aluminosilicate network of the glasses [31].

The network-forming SiO_4 units are described by their tetrahedral condensation as Q^n units, where n is the number of bridging oxygens (BOs) linked to the network former, ranging from 0 to 4. The ^{29}Si MAS NMR spectra (Fig. 2) all show rather broad featureless resonances, covering chemical shift regions for several different types of Q^n species, which reflect the amorphous nature of the glasses. The resonances can be characterized by their center of gravity (δ^{cg}) and linewidth (full width at half maximum) [31,36,37]. The ^{29}Si NMR spectra for the Zn-series (Fig. 2a) show that δ^{cg} slightly shifts towards higher chemical shifts with increasing Zn/Ca ratio. However, this shift is so small that the differences in structural connectivity must be rather small among the glasses of Zn-series.

The linewidths of the ^{29}Si resonances increase with increasing Zn, suggesting an increased distortion of the local environments for the SiO_4 tetrahedra [33], being consistent with Zn being primarily associated with NBOs (Fig. 3). This tendency of Zn to be near SiO_2 is confirmed by the formation of Zn_2SiO_4 in Zn30 and Zn40, and by the fact that the main stable phase is Zn_2SiO_4.

Sharp peaks in the ^{29}Si MAS NMR spectrum of the Zn40 glass indicate

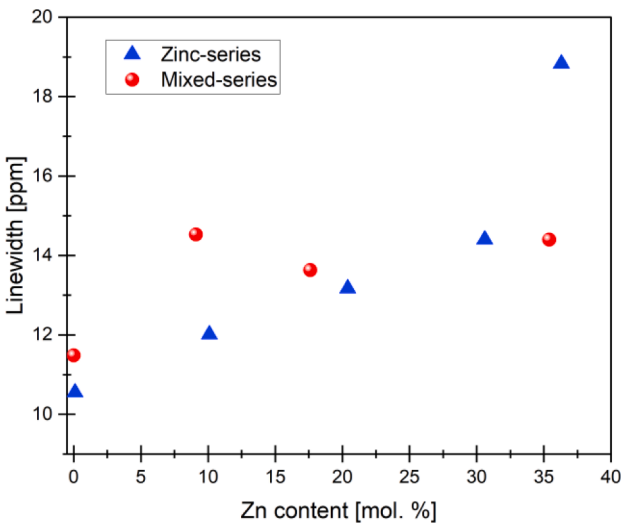

Fig. 3. Dependence of the linewidths on the mol% of zinc in the glasses for the zinc series (blue dots) and the mixed series (orange dots).

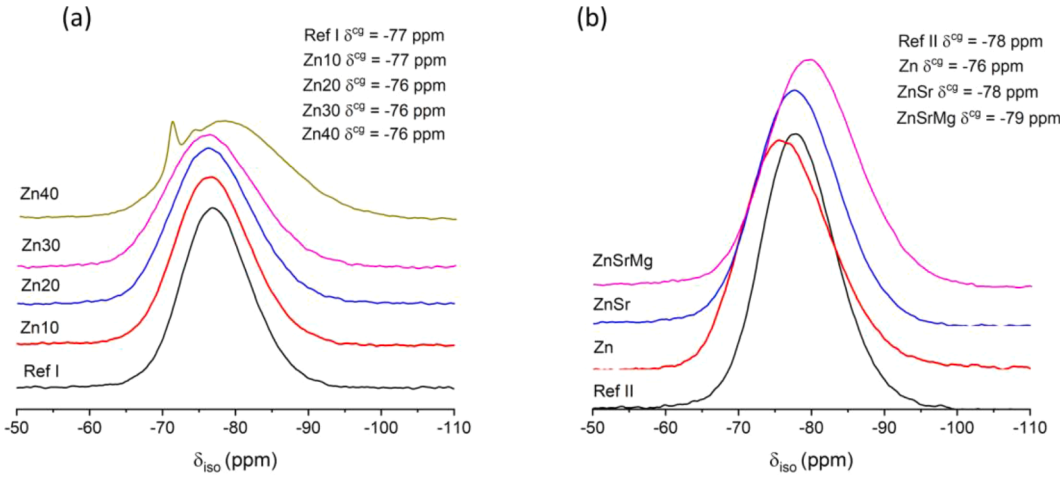

Fig. 2. ^{29}Si MAS NMR spectra for the glasses in the (a) zinc-series [22] and (b) mixed-series. Intensities have been normalized for the weight percentage of Si contained in each glass.

one or more crystalline phases containing silicon such as Zn_2SiO_4. However, the presence of gehlenite in the Zn10 glass as observed by XRD cannot be verified by NMR, possibly due to overlap with the main signals from the amorphous network. Amorphous materials have a disordered structure, and a broad NMR signal will appear due to the overlapping signals from the atoms within the material experiencing slightly different magnetic fields. This is not the case for crystalline materials, where the ordered structure ensures equal excitation of the atoms covering the same position within the crystal framework. Hence, crystalline materials give a well defined signal when measured by NMR [33]. The high content of crystalline phases in the Zn40 glass is also observed after the synthesis, as the glass appeared white in different areas [22]. This increased crystallization tendency, when increasing Ca substitution by Zn, is consistent with the low difference between T_c and T_g observed for Zn40 [38].

The ^{29}Si MAS NMR spectra of the mixed-series show a shift of δ^{cg} for the four glasses, though no clear trend is observed (Fig. 2b). The chemical shift depends on the Si environment and is as such affected by network connectivity, as well as by next-nearest-neighboring atoms. As the NBO/T values, and thus the network connectivity, are different for the four glasses in the mixed-series, it is difficult to conclude how the different modifier ions in the glasses affect the Si environment. Nevertheless, it is clear that the shift observed in the δ^{cg} of the different glasses cannot be solely explained by the calculated NBO/T values.

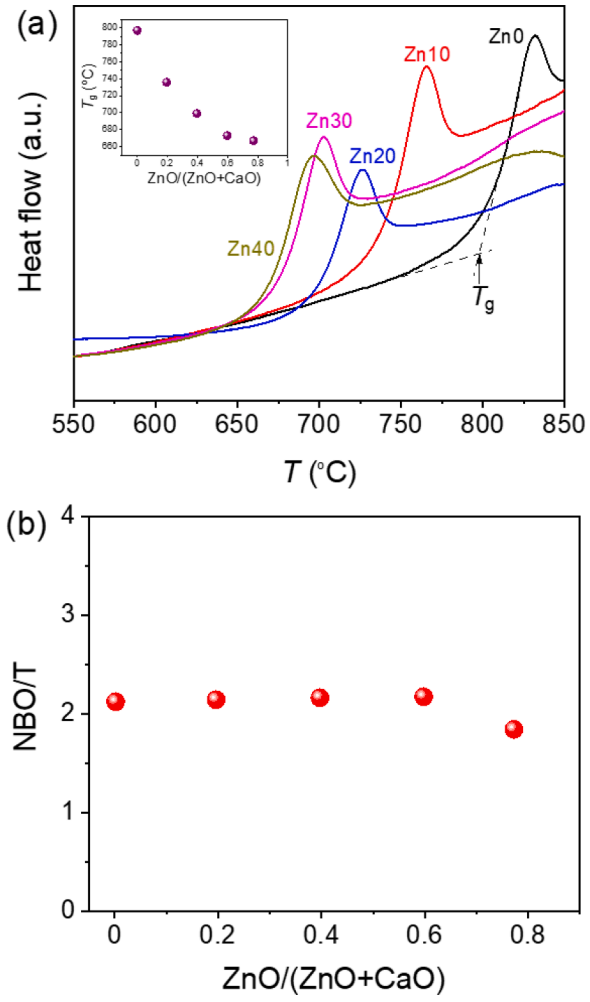

Fig. 4. (a) DSC upscans carried out on Zn-series glasses at the rate of 20°C/min, and an example about how to determine the glass transition temperature (T_g) [22]; inset: dependence of T_g on the amount of the substituted zinc fraction for CaO, i.e., ZnO/(ZnO+CaO). (b) NBO/T as a function of the molar ratio between ZnO and ZnO+CaO in the Zn-series.

Fig. 4a shows a striking phenomenon, i.e., the T_g value drastically decreases with a gradual substitution of ZnO for CaO, and drops even by 130°C when ZnO replaces about 80% of CaO content. It is also seen, in the inset of Fig. 4, that the rate of the T_g drop with Zn content decreases at increasing Zn content. The trend is well-fitted by the decay equation:

$$T_g = T_{g0}\cdot\exp\left(-k\frac{\mathrm{ZnO}}{\mathrm{ZnO}+\mathrm{CaO}}\right) \quad (3)$$

where T_{g0} is the value of T_g for no zinc (793.7°C), with k=0.2733 under the values for the abscissa in the inset of Fig. 4a experienced in this work. The statistical coefficient of determination is R^2=0.9782.

It is generally believed that T_g of an oxide glass is controlled by two structural factors: the network connectivity and the cationic field strength [39]. Thus, to find the origin of the significant T_g drop induced by Zn, the network connectivity is determined by calculating NBO/T (Fig. 4b) according to Eq. (1). The data in Fig. 4b indicate that NBO/T, and so the network connectivity, varies only slightly with increasing the ZnO/(ZnO+CaO) ratio. This implies that T_g drop has no connection with network connectivity. However, considering the ionic size difference between Zn and Ca, the field strength of Zn must be larger than that of Ca [34]. Hence, compared with Ca ions, Zn ions more strongly interact with NBOs in the primary network (structural skeleton) constituted by [AlO_4] and [SiO_4] tetrahedra, and thereby weaken the primary network, therefore lowering T_g significantly.

Moreover, the T_g drop can be explained in terms of the network rigidity theory, specifically the temperature-dependent bond constraint theory [40,41]. Accordingly, T_g decreases with a decrease of the number of the constraints, i.e., an increase of the atomic degree of freedom in a topological network. It is known that, for oxide glass systems like our present ones, the number of linear bond constraints decreases with an increase of NBO/T [42,43]. However, NBO/T in the investigated glass system remains almost unchanged with substituting Zn for Ca (Fig. 4b), implying that the number of the linear constraints does not undergo any detectable change. To understand why T_g sharply drops with substituting Zn, the sub-network consisting of modifier-NBO bonds needs to be considered. Two previous studies introduced the constraint number of the modifying ion sub-network [44] and the strength of modifier constraints [45], respectively, into calculation of the network rigidity. Each modifier contributes to the rigidity of the glass network, while the constraint strength is a measure of how strongly the modifiers are bound to the surrounding oxygens. Another study derived an extended topological model [46], which considered the effective number of intact constraints per modifying cation. This effective number is linearly related to the charge-to-distance ratio of the modifier-oxygen pair. In the present work, the substitution of Zn for Ca increases the effective number of the bond constraints in the modifying ion sub-network, due to the higher field strength of Zn. On the other hand, the increase of the rigidity of the sub-network weakens the primary network (structural skeleton) constituted by [AlO_4] and [SiO_4] tetrahedra, because Zn competes with Al and Si for NBOs. Consequently, the effective number of the intact constraints in the primary structural network becomes lower and, hence, T_g drops. In other words, the weakened constraints may be broken at lower onset temperature, so at lower T_g.

A sharp exothermic signal is observed for all substituted glasses around 850-975°C, indicating crystallization of the glass into one or more crystalline phases, whereas no crystallization occurs in the reference glass below 1000°C. The Zn40 glass has the lowest T_g value (see inset in Fig. 4a). Several crystallization signals are detected in the range of 850-1000°C. This may correspond to three crystallization events, indicating segregation or ordering in the glasses, even though only one amorphous phase was detected [47]. The low difference between T_g and T_c confirms a high crystallization tendency of the Zn40 glass, correlating with the crystallization occurring during quenching. Thus, at high replacements, the cooling rate used during the synthesis becomes critical

in determining the degree of crystallinity of the glasses.

The glasses were subjected to heat treatment at 1000°C, and Rietveld refinements of the XRD data reveal the presence of different crystalline phases. The formation of different crystal phases results from the different composition of the glasses and the changing ratios of divalent ions seems to cause a rearrangement of the network. The results for the Zn-series are shown in Fig. 5, where the crystal content (wt.%) is reported as a function of the Zn content (all references for the crystal structures are reported in the supplementary materials Table S.2). The presence of gehlenite and calcium silicate ($CaSiO_3$ 2M, parawollastonite) in the reference glass indicates the formation of a partially depolymerized region made of SiO_4 and (1/2Ca)AlO_4 tetrahedra, and a highly depolymerized region made of SiO_4 clusters rich in NBOs [47]. The introduction of a low amount of Zn^{2+} (10 mol. %) results in an incorporation of Zn^{2+} into the gehlenite structure with the formation of a calcium zinc silicate phase ($Ca_2(Al,Zn)(Al,Si)O_7$), and the formation of anorthite ($CaAl_2Si_2O_8$). The formation of anorthite occurs as a consequence of the decreasing Ca/Zn ratio and suggests that a highly polymerized region made of SiO_4 and (1/2Ca)AlO_4 tetrahedra exists in the glass. In contrast, the change in the gehlenite structure indicates that Zn substitutes Al in the partially polymerized region of SiO_4 and (1/2Ca)AlO_4 tetrahedra. Based on the gehlenite structure, Zn does not only substitute Al, but a minor amount of Zn also substitutes Ca. Zn can thereby take up both tetrahedral and octahedral configuration when present in amounts up to 10 mo. l%. The amount of gehlenite with embodied Zn^{2+} remains practically constant with decreasing Ca/Zn ratio and may be an indication of a limit for Zn incorporation in gehlenite. This limit seems to be 10 mol. % in the CAS system studied here. As the zinc content increases further, zinc silicate appears, and its amount increases as the Zn content is increased. The formation of zinc silicate suggests a depolymerized region similar as for the calcium silicate phase detected in the reference glass and indicates that Zn substitutes Ca in the glass structure at amounts above 10 mol. %.

The amount of gehlenite decreases with increasing Zn content, whereas the amount of anorthite increases. The increasing Zn^{2+} content is associated with a decreasing Ca^{2+} content, keeping the total M^{2+} ion concentration constant in the glass, and the change from gehlenite to anorthite is expected to be a result of the lower Ca content. The formation of Zn_2AlO_4 is not observed in the heat-treated glasses, even though it is the crystal phase forming in the quenched glasses. This suggests that the crystallization is highly dependent on the cooling rate and may suggest that the charge compensation of Al by Zn is not thermodynamically favorable [48,49].

The crystallization experiments may indicate a quasi-heterogeneous intermediate-range order [47] within the glasses (i.e., differences of local structures on the nanometer scale), resulting in the formation of several crystalline phases upon heat treatment, though only one glass transition is observed for the un-treated glasses. This will correlate with the observation of several crystallization peaks for CAS-Zn40.

The main phases in the heat treated mixed-series glasses were found to be zinc silicate (Zn_2SiO_4), calcium zinc silicate ($CaZnSiO_4$) and calcium zinc aluminum silicate ($CaZnAl_2SiO_7$), consistent with the phases observed for the zinc-series. A few reflections related to the phase calcium strontium aluminum silicate ($CaSrAl_2O_7$) were found in the XRD patterns of samples ZnSr and ZnSrMg. This suggests that also Sr^{2+} is incorporated in the gehlenite structure upon crystallization, and that it substitutes for Ca^{2+} as charge compensating ion for $[AlO_4]^-$.

3.2. Glass reactivity

During the dissolution tests, all glasses dissolved congruently, and no preferential release of Al or Si was observed. In this work, the dissolution degree of the glasses is quantified by the normalized amount of aluminum released from the glasses (X_{Al}) as described by Eq. (2). Fig. 6a and b show the X_{Al} values as a function of dissolution time, t, for both the Zn-series and the mixed-series, respectively.

The dissolution of the glasses in the Zn-series is observed to depend on the Zn content, as low contents (Ref I, Zn10) results in higher

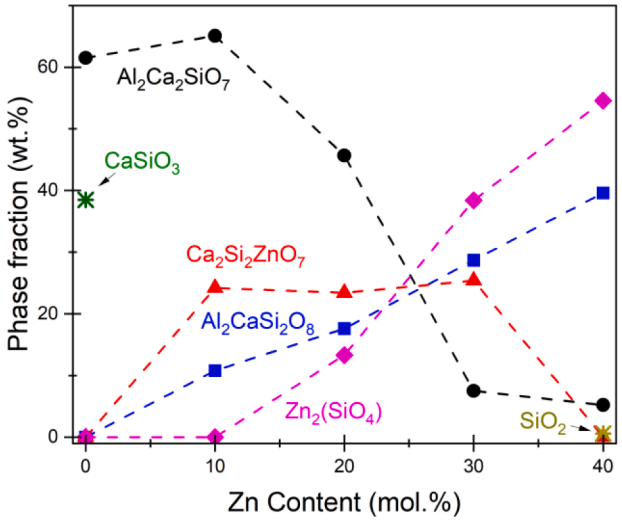

Fig. 5. Fraction of different phases (quantified using Rietveld refinement) for crystallized glasses in the Zn-series. Gehlenite ($Al_2Ca_2SiO_7$), wollastonite-2M ($CaSiO_3$), anorthite ($Al_2CaSi_2O_8$), calcium zinc silicate ($Ca_2Si_2ZnO_7$), zinc silicate ($Zn(SiO_4)$) and cristobalite (SiO_2). Dashed lines serve as a visual reference.

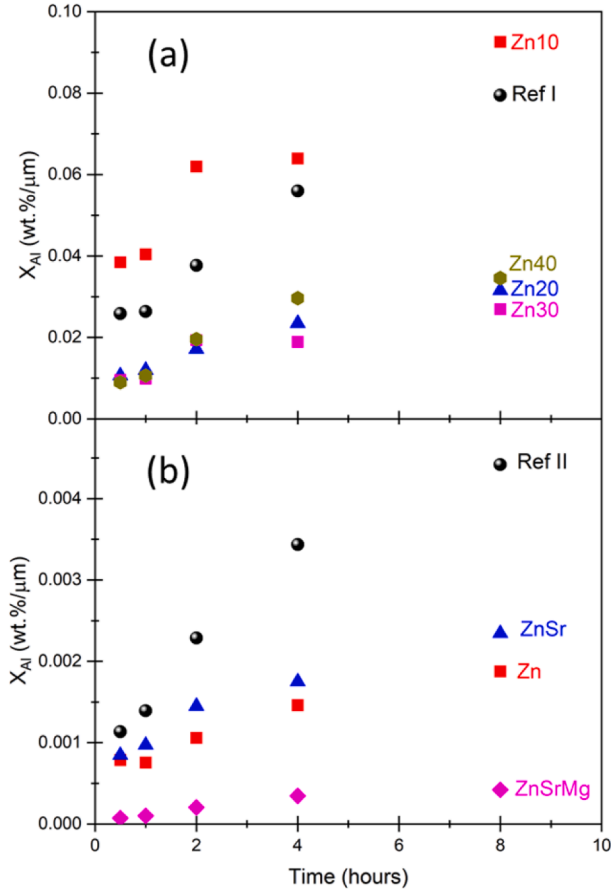

Fig. 6. Dissolution degrees of the glasses in (a) the Zn-series and (b) the mixed-series in terms of the normalized amount of Al released from the glasses (i.e., X_{Al} in Eq. (2)) as a function of dissolution time. Errors are estimated to be smaller than ± 1% for all samples. Note, that the scale of the y-axis is different in (a) and (b).

solubility during the first 8 hours in alkaline environment compared to higher contents (Zn20, Zn30, Zn40). The solubility may thereby be related to the structural rearrangements of the glasses indicated by the crystallization experiments (Fig. 5). A change in the crystalline phases forming was observed from Zn contents of 20 mol%, specifically the formation of Zn_2SiO_4.

The dissolution degrees of the glasses in the mixed-series also show a dependence on the substitution of Ca. The highest dissolution degree is observed for the reference glass followed by the ZnSr and Zn glasses, with Zn contents of 15 and 30 mol%, respectively. Thus, a similar trend occurs as observed for the Zn-series, indicating that Zn has a higher impact on the glass solubility than Sr. However, ZnSrMg shows a significantly lower dissolution degree, suggesting that also Mg lowers the solubility of the glasses to an even larger extent than Zn [50]. Additional studies are needed to conclude on the effect of Mg and Sr alone.

Although $X_{Al}(t)$ trends are increasing with dissolution time, the increase for X_{Al} appears more pronounced at shorter, rather than longer, t-values. Therefore, proposing the following relationship:

$$\frac{dX_{Al}(t)}{dt} = \frac{a}{t} \tag{4}$$

whose solution reads:

$$X_{Al}(t) = a \cdot \ln(t) + b \tag{5}$$

from Table 4 it is possible to see that this `"dissolution equation'' satisfactorily fits the experimental data, giving a tool to relate the dissolution degree with the dissolution time under the operating conditions experienced in this work.

The glasses solubility correlates with the pozzolanic test results (Figs. 7 and 8). Fig. 7a and b, respectively, show the amount of calcium hydroxide consumed by the reaction of the zinc-series glasses, and the bound water as a function of time. When the glasses dissolve, they react with calcium hydroxide to form hydrate phases. A decreasing amount of $Ca(OH)_2$ indicates an increasing extent of the pozzolanic reaction, therefore an increase in portlandite consumption. The reference is the most reactive sample up to 91 days, consistent with the increase in the amount of bound water related to C-S-H phases observed by TGA (Fig. 7b and supplementary materials Fig. S.4). Thereafter, similar Ca $(OH)_2$ consumptions are observed for the reference and the Zn10 sample. When comparing the $Ca(OH)_2$ contents in the five samples after 14 days, it is observed that the reactivity substantially decreases with increasing Zn contents in the glasses. This is consistent with the glass solubility, which decreases with increasing Zn contents in the glasses. Thus, Zn appears to have a retarding effect on the glass reactivity, especially concerning the pozzolanic reactivity of the glasses.

Fig. 8a shows the calcium hydroxide consumption as a function of time for the mixed-series samples. The increasing consumption of Ca $(OH)_2$ and bound water (Fig. 8b) with hydration time verifies that all samples are reactive. During the first 28 d, no significant reaction of the Zn containing glasses occur, and the reference sample is the most reactive, followed by ZnSrMg, ZnSr and Zn Thus, during the first 28 days, the pozzolanic reactivity decreases with Zn content in the glasses. A lower solubility of the substituted glasses was observed during the first 8 hours under alkaline conditions, which is consistent with the lower early reaction indicated by the pozzolanic tests; however, the high Ca $(OH)_2$ consumption detected after 182 days for all samples indicates that significant reaction does occur over time. As for the Zn-series, the reference glass is reacting significantly more than the substituted glasses. The low solubility of ZnSrMg is not reciprocated in the pozzolanic tests and the pozzolanic reactivity appears similar for all substituted glasses based on the Portlandite consumption. The higher bound water observed for the Zn glass at later ages may be a result of different hydrate phases forming.

Table 4
Fitting parameters for the dissolution Eq. (5), where dissolution degree and time have measure units as expressed in Fig. 5. Data for all the samples investigated. The statistical coefficient of determination, R^2, is reported as well.

Sample name	a	b	R^2
Ref I	0.0197	0.0314	0.9022
Zn10	0.0190	0.0463	0.9009
Zn20	0.0077	0.0136	0.9468
Zn30	0.0063	0.0126	0.8956
Zn40	0.0101	0.0137	0.9616
Ref II	0.0012	0.0017	0.9645
Zn	0.0004	0.0009	0.9109
ZnSr	0.0005	0.0011	0.9622
ZnSrMg	0.0001	0.0001	0.9616

3.3. Cement hydration

Based on the previous sections, Zn appears to have a retarding effect on the pozzolanic reactivity of the glasses. In order to test whether a retarding effect of Zn is also observed in blends with cement, Zn $(NO_3)_2{\cdot}6H_2O$ was added to the mixing water before mixing with cement, to ensure the immediate presence of Zn^{2+} ions. As seen in Fig. 9, a longer induction period is observed due to Zn addition, and the observed delay increases linearly with the increase of Zn concentration from 0 to 58 mM. As the reaction proceeds, the hydration rate is increased in both the acceleration and deceleration period for the blends containing zinc. This accelerating effect was also observed for pure C_3S in a study by Bazzoni et al. [51], where they detected that Zn in solution is homogenously incorporated in the C-S-H phase, which results in slightly thicker and clearly longer C-S-H needles (Fig. S.6 in the supplementary materials). The effect of zinc on the C-S-H growth rate is related to the accelerating effect observed by calorimetry. The cumulative heat response from the mixes with added $Zn(NO_3)_2{\cdot}6H_2O$ remains lower than the response from the reference paste also after 7 d, suggesting a significant impact on the early strength development.

Fig. 10 shows the TGA data of the PC reference sample and the sample mixed with Zn solution. The Portland reference sample (Fig. 10a) contains ettringite ($3CaO{\cdot}Al_2O_3{\cdot}3CaSO_4{\cdot}32H_2O$), portlandite and calcium carbonate. A small signal related to the presence of C-S-H is present as well. For the three cement blends prepared with $Zn(NO_3)_2{\cdot}6H_2O$, Sr $(NO_3)_2$, and $Mg(NO_3)_2$ dissolved in the mixing water, three additional peaks are observed by TGA as shown in Fig. 10b for the sample mixed with Zn solution. One is situated around 250°C and could be related to monocarbonate. The other two are situated around 170°C and between 450 and 550°C, respectively. These peaks occur during the first 28 d of hydration for the cement blend mixed with Zn solution (Fig. 10b), and during the first 7 days of hydration for the cement blends mixed with Zn-Sr solution and Zn-Sr-Mg solution, respectively. The peaks indicate the presence of calcium hydroxozincate hydrate with the peak around 175°C corresponding to the dehydration of zinc hydroxide, and the peak between 450 and 550°C corresponding to the dehydration of the Ca $(OH)_2$ present in this phase [52]. The formation of calcium hydroxozincate is known to retard the cement hydration [53,54], and its presence in the investigated blends correlates with the lower amount of bound water determined with increased Zn content (Fig. 11). A delayed portlandite formation was also observed for these blends by XRD (Fig. S.5), again consistent with the retarding effect of Zn on cement hydration.

The study of the cement mixed with nitrate solutions shows a retarding effect of Zn, whereas neither Sr nor Mg influence the hydration kinetics of the cement. Zinc has previously been used as a retarder in cement hydration [55]. Zinc reacts with the calcium ions released from the clinker minerals to form the calcium hydroxozincate hydrate ($Ca(Zn(OH)_3)_2{\cdot}2H_2O$) on the C_3S surface, delaying the precipitation of portlandite and C-S-H [56]. This may prolong the induction period until all Zn is consumed as no Ca is available to make C-S-H phases. Only after all zinc is fixed in this compound, additional dissolved calcium ions initiate

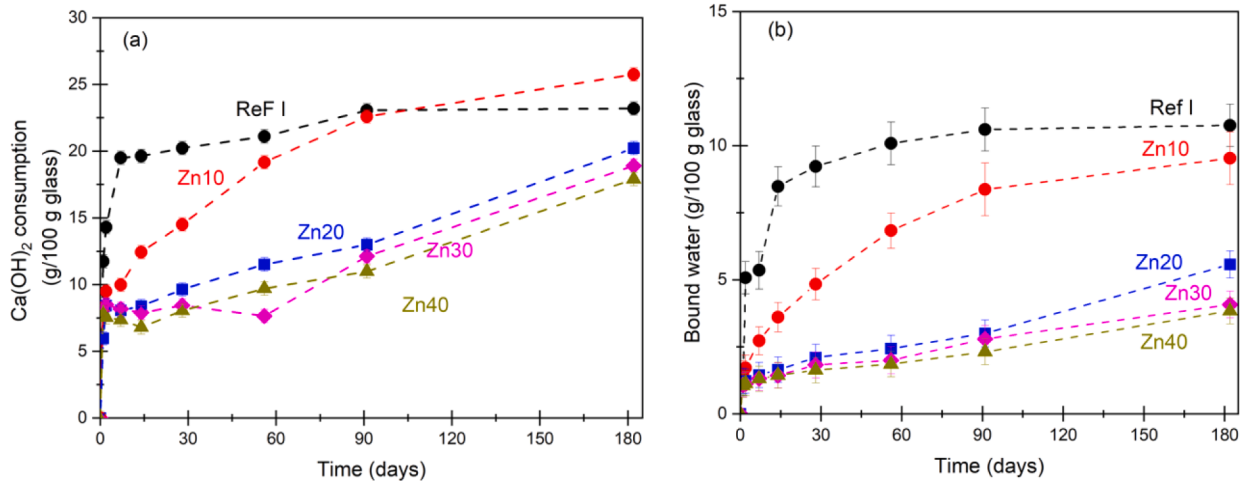

Fig. 7. Consumption of calcium hydroxide in the Zn-series glasses obtained as the difference between the initial amount of $Ca(OH)_2$ and what remains from the pozzolanic reaction vs. hydration time (a). Chemical bound water (b) vs. hydration time. The calculated amount of portlandite and water were normalized by 100 g of the initial glass amount.

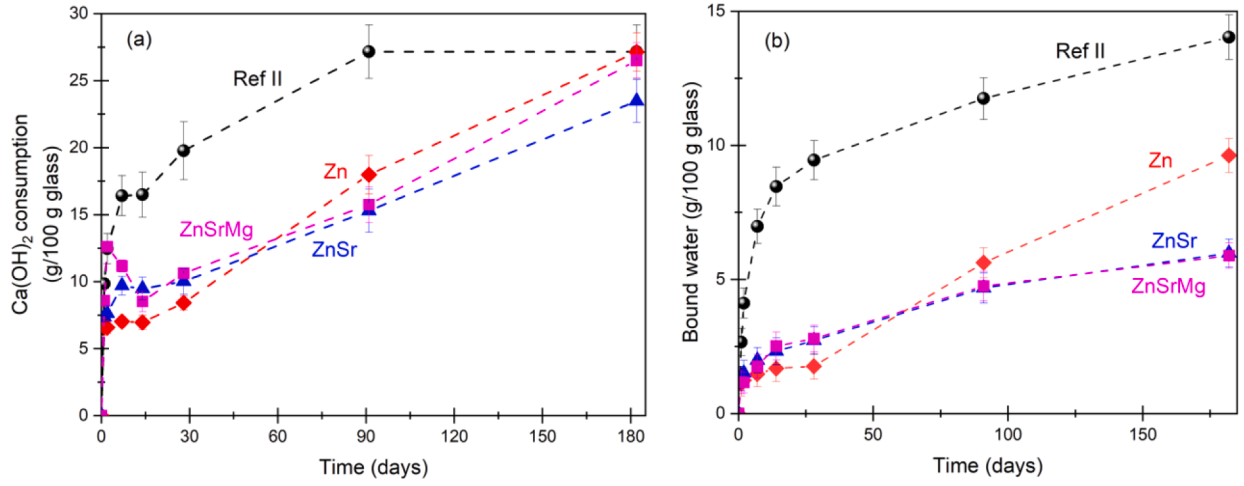

Fig. 8. Consumption of calcium hydroxide in the mixed-series glasses obtained as the difference between the initial amount of $Ca(OH)_2$ and what remains from the pozzolanic reaction vs. hydration time (a). Chemical bound water vs. hydration time (b). The calculated amount of portlandite and water were normalized by 100 g of the initial glass amount.

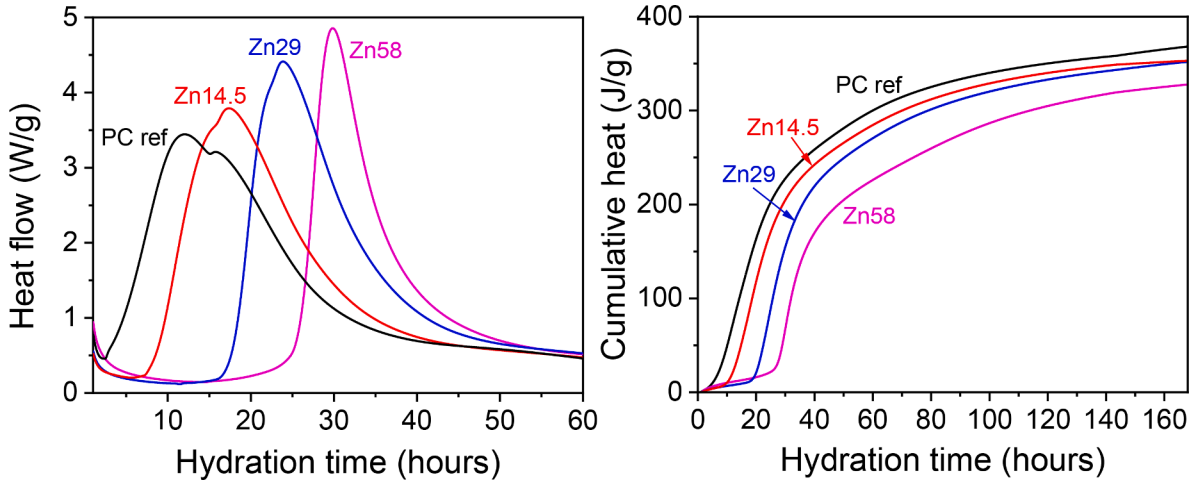

Fig. 9. Heat flow curves during the first 3 d of hydration (left) and cumulative heat flow up to 7 d of hydration (right). Cement systems: reference Portland CEM I 52.5 R cement ("PC ref"); cement blends CEM I 52.5 R mixed with $Zn(NO_3)_2{\cdot}6H_2O$ in demineralized water, with Zn concentrations of 14.5, 29 and 58 mM.

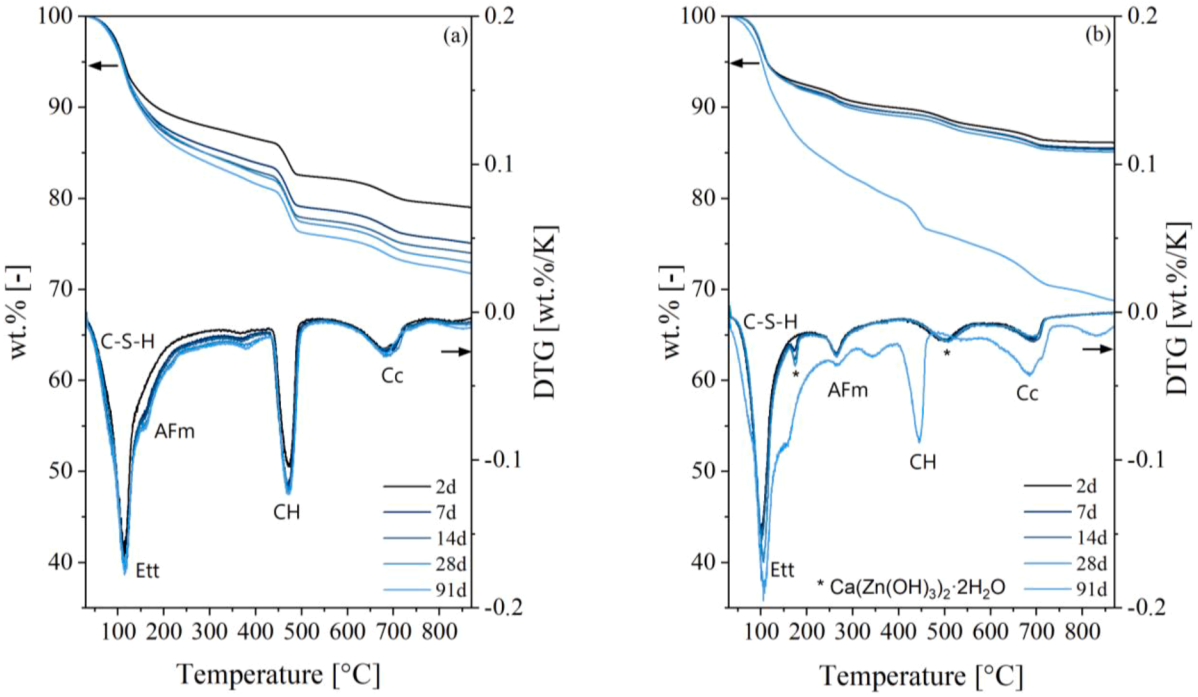

Fig. 10. Weight changes during heating at the rate of 20°C/min measured by TGA and differential weight changes, i.e., DTG for (a) reference Portland CEM I 52.5 R cement and (b) cement blends CEM I 52.5 R mixed with Zn solution.

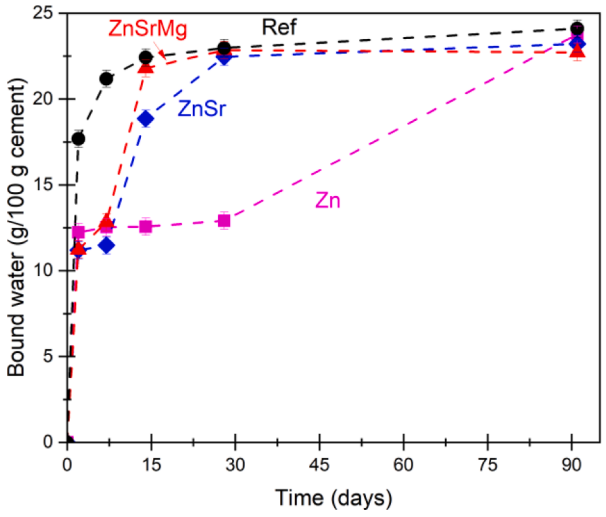

Fig. 11. Mass fraction of water present in the cement blends as a function of the hydration time. The mass of bound water was calculated by the mass loss in the temperature range between 30 and 550°C. The water mass was normalized by 100 g of dry cement.

the setting process during which the calcium hydroxozincate hydrate is decomposed [55,57,58]. However, also other mechanisms such as retardation by the formation of surface complexes due to the presence of Zn, might not be excluded. Multivalent cations are usually responsible of the formation of bi- or multinuclear surface complexes which cause the inhibition of the dissolution and consequently of the reactivity of the material [59]. In particular it has been seen in previous studies that Zn^{2+} ions can form surface complexes with both silanol and aluminol groups delaying the dissolution of amorphous aluminosilicate materials and so their reactivity [60–62].

XRD and TGA results confirm the presence of calcium hydroxozincate hydrate and show a later formation of portlandite with increasing Zn content in the pore solution, in agreement with the suggested mechanism described above.

5. Conclusions

All divalent ions were found to act primarily as modifiers in the glass structure, and their structural role in the studied glasses depends on the cation field strength, and so on their ionic radius. Zn (which is the ion with the higher CFS and so the lowest ionic radius) prefers to stay close to Si forming NBO. At high Zn/Ca ratios, however, Zn was detected near Al, indicating it acts to $[AlO_4]^-$ charge compensate despite its high CFS, due to a shortage of Ca ions. Sr and Mg simply substitute Ca in the glass network and compensate $[AlO_4]^-$ charge. Although the substitution of Ca with the divalent ions does not cause any detectable changes in the glass structure, it has been noticed that the T_g value drops drastically in a non-linear fashion when replacing CaO for ZnO. The origin of this striking phenomenon was clarified by considering the competition between the sub-constraints of network modifiers cation and the primary constraints of network formers.

All glasses were dissolved under alkaline conditions. Their dissolution degree depends on particle size, network connectivity and on the ionic radius of the different divalent ions. Zn and Mg, with the lowest ionic radius, have the highest CFS. This implies that they tend to form stronger bonds in the glass structure thus reducing its solubility, as observed during dissolution tests. Instead, Sr and Ca have a larger ionic radius and consequently a smaller CFS. When these ions are present (especially in the absence of Zn and Mg) there is a major formation of weaker bonds in the glass structure and thus the dissolution is more consistent. The pozzolanic reactivity of the glasses depends on the dissolution with the less soluble glasses also being the less reactive. Both glass series showed a decrease in reactivity with increased Zn content, but the presence of Sr and Mg did not influence the reactivity. The study on cement blends revealed a retarding effect of zinc on the cement hydration. A later portlandite formation was observed with increased zinc content in the pore solution and, furthermore, calcium hydroxozincate hydrate was detected by XRD. The formation of calcium hydroxozincate hydrate could be the cause for the retardation of both the pozzolanic

reactivity of the glasses and the cement hydration, as it affects the portlandite formation and thus the pH of the systems. Another cause of the retardation can be also related to the formation of bi- or multinuclear surface complexes due to the presence of Zn. Zn^{2+} ions are adsorbed onto amorphous aluminosilicate surface by forming a complex with the surface OH groups delaying the dissolution of this phase.

The current work indicated that alternative slags with a similar composition to the studied synthetic glasses are promising SCMs as they contribute to the hydration reaction in cementitious systems tough the retarding effect of Zn must be considered.

CRediT authorship contribution statement

Serena Mingione: Writing – original draft, Investigation. **Malene T. Pedersen:** Writing – original draft, Supervision, Funding acquisition, Conceptualization. **Søren S. Sørensen:** Writing – review & editing. **Frank Winnefeld:** Writing – review & editing, Supervision, Conceptualization. **Fabio Montagnaro:** Writing – review & editing, Supervision, Data curation. **Yuanzheng Yue:** Writing – review & editing.

Declaration of Competing Interest

The authors declare the following financial interests/personal relationships which may be considered as potential competing interests:

Malene Thostrup Pedersen reports financial support was provided by EU Framework Programme for Research and Innovation Marie Sklodowska-Curie Actions.

Data availability

Data will be made available on request.

Acknowledgements

The authors are grateful to Benedicte S. Halvorsen, Inga M. Tangen, Nanna L. Pallesen, Stine L. B. Hansen for their experimental work during their 7th Semester project at Aalborg University.

Bin Ma is thanked for ICP-OES measurements, Daniel Rentsch and Jørgen Skibsted are thanked for performing NMR measurements and the EMPAPOSTDOCS-II programme: Horizon 2020 Marie Skłodowska-Curie grant agreement number 754364 is acknowledged for funding.

Supplementary materials

Supplementary material associated with this article can be found, in the online version, at doi:10.1016/j.jnoncrysol.2023.122397.

References

[1] P. Monteiro, S. Miller, A. Horvath, Towards sustainable concrete, Nat. Mater. 16 (2017) 698–699.
[2] E. Gartner, Industrially interesting approaches to low-CO2 cements, Cem. Concr. Res. 34 (2004) 1489–1498.
[3] S. Telschow, F. Frandsen, J. Theisen, K. Dam-Johansen, Cement formation-A success story in a black box: high temperature phase formation of Portland cement clinker, Ind. Eng. Chem. Res. 51 (2012) 10983–11004.
[4] E. Gartner, T. Sui, Alternative cement clinkers, Cem. Concr. Res. 114 (2018) 27–39.
[5] E. Gartner, Potential improvements in cement sustainability, in: 31st Cement and Concrete Science Conference Novel Developments and Innovation in Cementitious Materials, Imperial College, London UK, September 2011, pp. 12–13.
[6] M.C.G. Juenger, F. Winnefeld, J.L. Provis, J.H. Ideker, Advances in alternative cementitious binders, Cem. Concr. Res. 41 (2011) 1232–1243.
[7] B. Lothenbach, K. Scrivener, R.D. Hooton, Supplementary cementitious materials, Cem. Concr. Res. 41 (2011) 1244–1256.
[8] M.C.G. Juenger, R. Siddique, Recent advances in understanding the role of supplementary cementitious materials in concrete, Cem. Concr. Res. 78 (2015) 71–80.
[9] J. Duchesne, Alternative supplementary cementitious materials for sustainable concrete structures: a review on characterization and properties, Waste Biomass Valorization 12 (2020) 1219–1236.
[10] M.C.G. Juenger, R. Snellings, S.A. Bernal, Supplementary cementitious materials: New sources, characterization and performance insights, Cem. Concr. Res 122 (2019) 245–273.
[11] M. Moesegaard, S.L. Poulsen, D. Herfort, M. Steenberg, L.F. Kirkegaard, J. Skibsted, Y.Z. Yue, Hydration of blended portland cements containing calcium-aluminosilicate glass powder and limestone, J. Am. Ceram. Soc. 95 (2012) 403–409.
[12] M. Moesegaard, D. Herfort, M. Steenberf, L.F. Kirkegaard, Y.Z. Yue, Physical performances of blended cements containing calcium aluminosilicate glass powder and limestone, Cem. Concr. Res. 41 (2011) 359–362.
[13] M. Reuter, Y. Xiao, U. Boin, Recycling and environmental issues of metallurgical slags and salt fluxes, in: VII International Conference on Molten Slags Fluxes and Salts, The South African Institute of Mining and Metallurgy, 2004, pp. 349–356.
[14] N.M. Piatak, M.B. Parsons, R.R.S. II, Characteristics and environmental aspects of slag: a review, Appl. Geochem. 57 (2015) 236–266.
[15] B. Li, B. Huo, R. Cao, S. Wang, Y. Zhang, Sulfate resistance of steam cured ferronickel slag blended cement mortar, Cem. Concr. Res. 122 (2019) 257–273.
[16] C. Siakati, A.P. Douvalis, V. Hallet, Y. Pontikes, Influence of CaO/FeO ratio on the formation mechanism and properties of alkali-activated Fe-rich slags, Cem. Concr. Res. 146 (2021) 106–466.
[17] V. Hallet, M. Pedersen, B. Lothenbach, F. Winnefeld, N.D. Belie, Y. Pontikes, Hydration of blended cement with high volume iron-rich slag from non-ferrous metallurgy, Cem. Concr. Res. 151 (2022) 106–624.
[18] D. Pan, L. Li, X. Tian, Y. Wu, N. Cheng, H. Yu, A review on lead slag generation, characteristics, and utilization, Reseour. Conserv. Recyl. 146 (2019) 140–155.
[19] P. Lv, C. Wang, B. Stevensson, Y. Yu, T. Wang, M. Edén, Impact of the cation field strenght on physical properties and structures of alkali and alkaline-earth borosilicatw glasses, Ceram. Intern. 48 (2022) 18094–18107.
[20] A. Schöler, F. Winnefeld, M.B. Haha, B. Lothenbach, The effect of glass composition on the reactivity of synthetic glasses, J. Am. Ceram. Soc. 100 (2017) 2553–2567.
[21] K. Mills, L. Youan, R.T. Jones, Estimating the physical properties of slags, J. S. Afr. Inst. Min. Metall. 10 (2011) 649–658.
[22] B. S. Halvorsen, I. M. Tangen, N. L. Pallesen, S. L. B. Rasmussen, The Influence of zinc ions on the structure of a model glass system resembling slag, student report of Aalborg University (2019).
[23] R. Snellings, J. Chwast, Ö. Cizer, N.D. Belie, Y. Dhandapani, P. Durdzinski, J. Elsen, J. Huafe, D. Hooton, C. Patapy, M. Santhanam, K. Scrivener, D. Snoeck, L. Steger, S. Tongbo, A. Vollpracht, F. Winnefeld, B. Lothenbach, RILEM TC-238 SCM recommendation on hydration stoppage by solvent exchange for the study of hydrate assemblages, Mater. Struct. 51 (2018) 111–123.
[24] B. O'Connor, M. Raven, Application of the Rietveld refinement procedure in assaying powdered mixtures, Powd. Diffr. 3 (1988) 2–6.
[25] D. Jansen, F. Götz-Neuhoeffer, C. Stabler, J. Neubauer, A remastered external standard method applied to the quantification of early OPC hydration, Cem. Concr. Res. 41 (2011) 602–608.
[26] K. Scrivener, R. Snellings, B. Lothenbach, X-Ray Powder Diffraction Applied to Cement, A Practical Guide to Microstructural Analysis of Cementitious Materials, CRC Press, Taylor & Francis Group, 2016, pp. 107–175.
[27] D. Massiot, F. Fayon, M. Capron, I. King, S.L. Calvé, B. Alonso, J. Durand, B. Bujoli, Z. Gan, G. Hoatson, Modelling one- and two-dimensional solid state NMR spectra, Magn. Reson. Chem. 40 (2002) 70–76.
[28] JB d'Espinose de Lacaillerie, C. Fretigny, D. Massiot, MAS NMR spectra of quadrupolar nuclei in disordered solids: the Czjzek model, J. Magn. Reson. 192 (2008) 244–251.
[29] D.R. Neuville, L. Cormier, D. Massiot, Al environment in tectosilicate and peraluminous glasses: a 27Al MQ-MAS NMR, Raman, and XANES investigation, Geochim. Cosmochim. Acta 68 (2004) 5071–5079.
[30] R. Snellings, Solution-controlled dissolution of supplementary cementitious material glasses at pH 13: the effect of solution composition on glass dissolution rates, J, Am. Ceram. Soc. 96 (2013) 2467–2475.
[31] S. Nie, R.M. Thomsen, J. Skibsted, Impact of Mg substitution on the structure and pozzolanic reactivity of calcium aluminosilicate (CaO-Al2O3-SiO2) glasses, Cem. Concr. Res. 138 (2020) 106–231.
[32] S.K. Lee, J.F. Stebbins, The degree of aluminum avoidance in aluminosilicate glasses, Am. Min. 84 (1999) 937–945.
[33] R.M. Thomsen, J. Skibsted, Y. Yue, The charge-balancing role of calcium and alkali ions in pre-alkaline aluminosilicate glasses, J. Phys. Chem. 122 (2018) 3184–3195.
[34] K. Kanehashi, Structural roles of calcium in alkaline-earth aluminosilicate glasses by solid-state 43Ca, 17O and 27Al NMR, Solid State Nucl. Magn. Reson. 84 (2017) 158–163.
[35] K. Januchta, M. Bauchy, R.E. Youngman, S.J. Rzoska, M.Smedskjaer M.Bockowski, Modifier field strength effects on densification behavior and mechanical properties of alkali aluminoborate glasses, Phys. Rev. Mater. 1 (2017) 63–603.
[36] J.B. Murdoch, J.F. Stebbins, I.S.E. Carmichael, High-resolution 29Si NMR study of silicate and aluminosilicate glasses: the effect of network-modifying cations, Am. Mineral. 70 (1985) 332–343.
[37] S. Kucharczyk, M. Zajac, C. Stabler, R.M. Thomsen, M.B. Haha, J. Skibsted, J. Deja, Structure and reactivity of synthetic CaO-Al2O3-SiO2 glasses, Cem. Concr. Res. 120 (2019) 77–91.
[38] M. Saad, M. Poulain, Glass forming ability criterion, Mater. Sci. Forum 19-20 (1987) 11–18.
[39] Q. Zheng, M. Potuzak, J.C. Mauro, M.M. Smedskjaer, R.E. Youngman, Y. Yue, Composition-structure-property relationships in boroaluminosilicate glasses, J. Non-Cryst. Solids 358 (2012) 993–1002.

[40] P.K. Gupta, J.C. Mauro, Composition dependence of glass transition temperature and fragility. I. A topological model incorporating temperature-dependent constrains, J. Chem. Phys. 130 (2009) 094–503.
[41] M.M. Smedskjaer, J.C. Mauro, S. Sen, Y. Yue, Quantitative design of glassy materials using temperature-dependent constraint theory, Chem. Mater. 22 (2010) 5358–5365.
[42] A.K. Varshneya, Fundamentals of inorganic glasses, society of glass technology, Sheffield (2006).
[43] J. Kjeldsen, M.M. Smedskjaer, J.C. Mauro, R.E. Youngman, L. Huang, Y. Yue, Mixed alkaline earth effect in sodium aluminosilicate glasses, J. Non-Cryst. Solids 369 (2013) 61–69.
[44] C. Hermansen, J.C. Mauro, Y. Yue, A model for phosphate glass topology considering the modifying ion sub-network, J. Chem. Phys. 140 (2014) 154–501.
[45] B.P. Rodrigues, L. Wondraczek, Cationic constraint effects in metaphosphate glasses, J. Chem. Phys. 140 (2014) 214–501.
[46] C. Hermansen, B.P. Rodrigues, L. Wondraczek, Y. Yue, An extended topological model for binary phosphate glasses, J. Chem. Phys. 141 (2014) 244–502.
[47] M. Moesegaard, R. Keding, J. Skibsted, Y. Yue, Evidence of intermediate-range order eterogeneity in calcium aluminosilicate glasses, Chem. Mater. 22 (2010) 4471–4483.
[48] S. Petrescu, M. Constantinescu, E.M. Anghel, I. Atkinson, M. Olteanu, M. Zaharescu, Structural and physico-chemical characterization of some soda lime zinc alumino-silicate glasses, J. Non-Cryst. Solids 358 (2012) 3280–3288.
[49] L. Cornier, L. Delbes, B. Baptiste, V. Montouillout, Vitrification, crystallization behavior and structure of zinc aluminosilicate glasses, J. Non-Cryst. Solids 555 (2021), 120609.
[50] D.R. Neuville, L. Cormier, V. Montouillout, P. Florian, F. Millot, J.C. Riflet, D. Massiot, Structure of Mg- and, Mg/Ca aluminosilicate glasses: ^{27}Al NMR and Raman spectroscopy investigations, Am. Mineral. 93 (2008) 1721–1731.
[51] A. Bazzoni, S. Ma, Q. Wang, X. Shen, M. Cantoni, K.L. Scrivener, The effect of magnesium and zinc ions on the hydration kinetics of C3S, J. Am. Ceram. Soc. 97 (2014) 3684–3693.
[52] S. Wang, Z. Yang, L. Zeng, Study of calcium zincate synthesized by solid phase synthesis method without strong alkali, Mater. Chem. Phys. 112 (2008) 603–606.
[53] W. Lieber, Influence of zinc oxide on the setting and hardenin of Portland cement, Zement-Kalk-Gips 20 (1967) 91–95.
[54] G. Arliguie, J.P. Ollivier, J. Grandet, Etude de l'effet retardateur du zinc sur l'hydratation de la pate de ciment Portland, Cem. Concr. Res. 12 (1982) 79–86.
[55] F. Liebeau, A. Amel-Zdeh, The Crystal Structure of Ca(Zn2(OH)6)*2H2O, a Retarder in the Setting of Portland Cement, Kristall & Technik, 1972, pp. 221–227.
[56] P. Siler, I. Kolarova, R. Novotny, J. Masiko, J. Porizka, J. Bednarek, J. Svec, T. Opravil, Application of isothermal and isoperibolic calorimetry to assess the effect of zinc on cement hydration, J. Therm. Anal. Calorim. 133 (2018) 27–40.
[57] Q. Chen, M. Tyrer, C. Hills, X. Yang, P. Carey, Immobilisation of heavy metal in cement-based solidification/stabilisation: a review, Waste Manag. 29 (2009) 390–403.
[58] F.F. Ataie, M.C. Juenger, S.C. Tay, Comparison of the retarding mechanisms of zinc oxide and sucrose on cement hydration and interactions with supplementary cementitious materials, Cem. Concr. Res. 72 (2015) 128–136.
[59] W. Stumm, Reactivity at the mineral-water interface: dissolution and inhibition, Colloids Surf. A 120 (1997) 143–166.
[60] A. Miyazaki, M. Matsuo, M. Tsurumi, Surface-complex formation between Zn ions and amorphous aluminosilicate in acquatic system, J. Colloid Interface Sci. 177 (1996) 335–338.
[61] A.V. Kostin, L.V. Mostalygina, O.I. Bukhtoyarov, The Mechanism of adsorption of zinc and cadmium ions onto bentonite clay, Prot. Met. Phys. Chem. Surf. 51 (2015) 773–778.
[62] A. Miyazaki, I. Balint, Y. Nakano, Solid-liquid interfacial reaction of Zn^{2+} ions on the surface of amorphous aluminosilicates with various Al/Si ratios, Geochim. Cosmochim. Acta 67 (2003) 3833–3844.